Molecular Therapy
Original Article

ZFN-mediated *in vivo* gene editing in hepatocytes leads to supraphysiologic α-Gal A activity and effective substrate reduction in Fabry mice

Silvere Pagant,[1,3] Marshall W. Huston,[2,3] Luciana Moreira,[1] Lin Gan,[1] Susan St Martin,[2] Scott Sproul,[2] Michael C. Holmes,[2] Kathleen Meyer,[2] Thomas Wechsler,[2] Robert J. Desnick,[1] and Makiko Yasuda[1]

[1]Department of Genetics and Genomic Sciences, Icahn School of Medicine at Mount Sinai, New York, NY 10029, USA; [2]Sangamo Therapeutics, Inc., Brisbane, CA 94005, USA

Fabry disease, a lysosomal storage disorder resulting from the deficient activity of α-galactosidase A (α-Gal A), is characterized by cardiac, renal, and/or cerebrovascular disease due to progressive accumulation of the enzyme's substrates, globotriaosylceramide (Gb3) and globotriaosylsphingosine (Lyso-Gb3). We report here the preclinical evaluation of liver-targeted *in vivo* genome editing using zinc-finger nuclease (ZFN) technology to insert the human α-galactosidase A (h*GLA*) cDNA into the albumin "safe harbor" locus of Fabry mice, thereby generating an albumin-α-Gal A fusion protein. The mature α-Gal A protein is secreted into the circulation for subsequent mannose-6-phosphate receptor-mediated tissue uptake. Donor vector optimization studies showed that replacing the h*GLA* cDNA signal peptide sequence with that of human iduronate 2-sulfatase (*IDS*) achieved higher transgene expression. Intravenous adeno-associated virus (AAV) 2/8-mediated co-delivery of the *IDS*-h*GLA* donor and ZFNs targeting the albumin locus resulted in continuous, supraphysiological plasma and tissue α-Gal A activities, which essentially normalized Gb3 and Lyso-Gb3 levels in key tissues of pathology. Notably, this was achieved with <10% of hepatocytes being edited to express h*GLA*, occurring mostly via non-homologous end joining (NHEJ) rather than homology-directed repair (HDR). These studies indicate that ZFN-mediated *in vivo* genome editing has the potential to be an effective one-time therapy for Fabry disease.

INTRODUCTION

Fabry disease (OMIM: 301500) is an X-linked lysosomal storage disorder due to pathogenic mutations in the α-galactosidase A gene (*GLA*) that encodes the exogalactosyl hydrolase, α-galactosidase A (α-Gal A; GenBank: NP_000160.1).[1] Absent or markedly deficient α-Gal A activity leads to the progressive systemic accumulation of the enzyme's major glycosphingolipid substrate, globotriaosylceramide (Gb3), and its soluble deacylated derivative, globotriaosylsphingosine (Lyso-Gb3), especially in the lysosomes of vascular endothelial cells, renal cells (i.e., epithelial, endothelial, and mesangial), and cardiomyocytes.[2–5] Males with the type 1 classic phenotype have essentially no α-Gal A activity and present in childhood or adolescence with acroparesthesias, angiokeratomas, hypohidrosis, and a characteristic corneal dystrophy.[1,6,7] In the absence of treatment, the progressive deposition of the substrates leads to cardiac, renal, and/or cerebrovascular disease and early demise, typically in the fourth or fifth decade of life. In contrast, type 2 later-onset males have α-Gal A mutations that encode low levels of enzymatic activity and have very little, if any, endothelial vascular involvement and therefore lack the early manifestations of the type 1 males. These patients typically develop kidney and/or cardiac disease in the fourth to sixth decades of life.[8–10] The clinical severity of female heterozygotes varies and is determined primarily by X-chromosome inactivation.[11]

Since 2001, the approved therapy for patients with type 1 or 2 Fabry disease has been enzyme-replacement therapy (ERT), which involves intravenous infusions of recombinant human α-Gal A delivered to tissue lysosomes via mannose-6-phosphate (M6P) receptor-mediated endocytosis.[12–14] Although ERT is effective, especially if initiated early in the course of the disease,[13,15–17] it necessitates lifelong 2- to 4-h infusions every 2 weeks. In addition, a significant percentage of type 1 classic males make antibodies to the therapeutic enzyme, which, if neutralizing, can decrease the amount of effective enzyme.[18,19] Recently, an oral pharmacological chaperone therapy (1-deoxygalactonojirimycin [DGJ], migalastat) was approved for the treatment of Fabry disease in the United States and other parts of the world, but most of the *GLA* mutations responsive to this approach cause the type 2 phenotype.[20–22] Therefore, a long-lasting treatment that is effective for both type 1 and 2 Fabry patients is desirable.

In vivo genome editing is an approach that uses programmable nucleases to generate a double-strand break (DSB) at a specific chromosomal locus, which, in mammalian cells, induces two major DNA

Received 8 September 2020; accepted 22 March 2021;
https://doi.org/10.1016/j.ymthe.2021.03.018.

[3]These authors contributed equally

Correspondence: Makiko Yasuda, MD, PhD, Assistant Professor, Department of Genetics and Genomic Sciences, Icahn School of Medicine at Mount Sinai, 1425 Madison Ave, Box 1498, New York, NY 10029, USA.
E-mail: makiko.yasuda@mssm.edu

repair mechanisms.[23–25] Non-homologous end joining (NHEJ) is a highly efficient repair process that, although most repair reactions occur with high fidelity, can also introduce small insertions and deletions (indels) while ligating the two ends of the DNA during repair. Homology-directed repair (HDR) is a high-fidelity process that repairs by copying a sister chromatid or exogenous DNA template (e.g., donor vector). By exploiting these endogenous DNA repair mechanisms, the genome can be edited to disrupt gene function, correct specific mutations, or introduce a therapeutic transgene into a "safe harbor" locus for *in vivo* protein replacement. Heterodimeric zinc-finger nucleases (ZFNs) were the first of the widely applicable programmable nucleases and consist of a DNA-binding zinc-finger protein (ZFP) domain fused to the catalytic domain of the *FokI* endonuclease.[26–28] Recent advancements in designing highly specific ZFPs, combined with the use of viral vectors as a delivery platform, have facilitated the application of this technology for therapeutic *in vivo* genome editing in patients.

Here, we report preclinical studies of a liver-targeted *in vivo* ZFN-mediated genome editing strategy in an α-Gal A knockout mouse model (*Gla* KO mouse) of Fabry disease that progressively accumulates Gb3 and Lyso-Gb3 in the plasma and tissues.[29] Two obligate heterodimeric ZFNs targeting intron 1 of the murine albumin (m*Alb*) gene and a donor vector carrying a codon-optimized human *GLA* (h*GLA*) cDNA were individually packaged into adeno-associated viral (AAV) 2/8 vectors and intravenously co-administered, to permanently insert the h*GLA* transgene into the m*Alb* intron 1 safe harbor locus.[30–32] A single administration of the h*GLA* donor and ZFN vectors resulted in markedly increased expression of appropriately glycosylated, active α-Gal A and normalized substrates in key tissues of pathological significance in the Fabry mice.

RESULTS

AAV2/8-mediated delivery of obligate heterodimeric ZFNs and a signal-peptide-less h*GLA* transgene results in misfolded α-Gal A enzyme in HepG2 cells and Fabry mice

Three AAV2/8 vectors were co-administered, two of which encode obligate heterodimeric ZFNs targeting intron 1 of the m*Alb* locus (designated ZFN vectors) and one that contains the therapeutic h*GLA* cDNA flanked by homology arms (HAs) to the targeted *Alb* locus (designated h*GLA* donor; Figure 1A). Co-transduction of the three vectors results in the permanent insertion of the h*GLA* transgene into the first intron of the m*Alb* gene. Due to an added splice acceptor (SA) site 5′ of the h*GLA* cDNA, activation of the *Alb* promoter leads to a chimeric transcript including exon 1 of the *Alb* gene, which contains the secretory signal peptide, and the h*GLA* cDNA (Figure 1A). Subsequent translation and post-translational processing of the albumin-α-Gal A fusion protein results in the production of mature, glycosylated α-Gal A enzyme that is secreted at high levels into the plasma for uptake by various tissues via the M6P-receptor-mediated uptake system.

Initial studies were performed using a donor construct containing a codon-optimized h*GLA* cDNA that lacked sequences encoding the 31-amino-acid h*GLA* signal peptide (designated nosp-h*GLA* donor; Figure 1A). With this donor design, the resulting mature α-Gal A enzyme has two additional N-terminal amino acids (EA in mouse, DA in human HepG2 cells) that remain following cleavage of the albumin signal peptide (Figure 1A, denoted by a star). Co-transduction of HepG2 cells with this donor and ZFN vectors targeting human *ALB* intron 1 resulted in intracellular α-Gal A activities that were ∼2- to 5-fold higher than mean endogenous levels in three independent gene-edited clones (Figure 1B). Addition of the chemical chaperone, DGJ, into the cell culture medium induced dose-dependent increases in intracellular α-Gal A activities in all three clones, reaching values that were up to ∼12-fold higher than mean endogenous levels (Figure 1B).

Similarly, Fabry mice that were co-administrated the nosp-h*GLA* donor (1.2E+12 vector genomes per mouse [vg/mouse]) and the m*Alb*-targeted ZFN vectors (1.5E+11 vg/mouse each) had mean plasma α-Gal A activity that was ∼2-fold higher than control Fabry mice administered just the nosp-h*GLA* donor (i.e., no ZFN vector; Figure 1C). ∼45% of the *Alb* loci had indels, indicating significant ZFN activity and subsequent repair via NHEJ in the livers of the mice treated with all three vectors (Table 1). When a subset of treated mice was administered daily oral doses of DGJ from 30 days post-injection onward, mean plasma α-Gal A activity increased up to ∼13-fold over that of the donor-only controls, achieving levels comparable to wild-type mice (Figure 1C).

Taken together, these findings suggested that low α-Gal A activity observed in the treated mice was not due to inefficient genome editing but rather due to misfolding of the liver-expressed α-Gal A enzyme. We hypothesized that the protein misfolding may be caused by the two m*Alb* signal peptide amino acids that remained on the N-terminus of the α-Gal A enzyme following cleavage of the *Alb* signal peptide (Figure 1A). Thus, subsequent efforts evaluated whether addition of a cleavable signal peptide sequence immediately 5′ of the h*GLA* cDNA would lead to efficient cleavage of these two amino acids, resulting in properly folded, active α-Gal A enzyme.

Addition of a signal peptide sequence to the h*GLA* transgene enhances α-Gal A activity and achieves effective substrate clearance in Fabry mice

To assess whether the addition of a cleavable signal peptide sequence to the h*GLA* transgene results in higher α-Gal A expression, the nosp-h*GLA* donor was modified to include the h*GLA* signal peptide sequence (*GLA*sp), either alone (*GLA*sp-h*GLA*) or in combination with a modified GCCACC Kozak sequence (Kozak-*GLA*sp-h*GLA*) or a 2A self-cleaving peptide[33] (T2A-*GLA*sp-h*GLA*), or the human iduronate 2-sulfatase (*IDS*) signal peptide (PPPRTGRGLLWL GLVLSSVCVALG, *IDSsp*-h*GLA;* Figure 2A). The Kozak sequence was incorporated to drive translation from the *GLA*sp, while the 2A self-cleaving peptide was included to enhance cleavage of the two *Alb* signal peptide residues.

Fabry mice administered ZFN vectors (1.5E+11 vg/mouse each) and the *GLA*sp-containing donors (1.2E+12 vg/mouse), regardless of

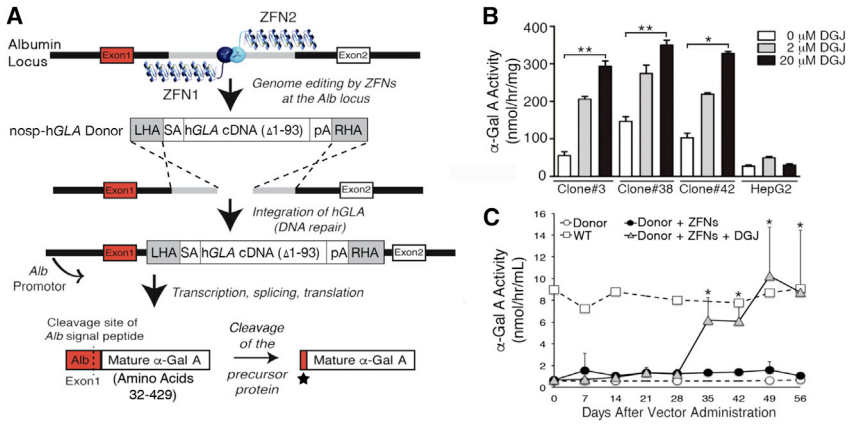

Figure 1. Signal-peptide-less h*GLA* transgene results in only modest increases of α-Gal A activity *in vitro* and *in vivo*

(A) Schematic representation of the *Alb* intron 1 *in vivo* protein replacement strategy. The initial nosp-h*GLA* donor consisted of a human factor IX splice acceptor (SA), a codon-optimized h*GLA* cDNA lacking the signal peptide (nucleotides 1–93; △ 1–93), and a poly A cassette (pA) flanked by *Alb* intron 1 homology arms (left [LHA] and right homology arm [RHA]). Following transgene integration into the *Alb* locus via DNA repair, transcription, splicing, and translation of the modified locus give rise to a chimeric protein containing exon 1 of the *Alb* gene (depicted in red), which includes the secretory signal peptide, followed by the signal-peptide-less α-Gal A enzyme. Cleavage of the *Alb* signal peptide results in mature α-Gal A enzyme (amino acids 32–429) with two additional N-terminal amino acids, DA in human and EA in mouse (denoted by a star), which are contributed by the *Alb* signal peptide. (B) Intracellular α-Gal A activities in three independent, stably modified HepG2 clones (clones #3, 38, and 42) using the nosp-h*GLA* donor. DGJ was added into the culture medium at a final concentration of 2 or 20 μmol/L and incubated for 24 h. Data for untransduced HepG2 cells are shown for reference. Presented data are means ± SDs (n = 3). The α-Gal A activities of each clone, before (0 μM DGJ) versus after addition of 20 μM DGJ were compared to assess statistical significance. *$p < 0.05$ and **$p < 0.01$. (C) Time course of plasma α-Gal A activities of Fabry male mice injected with a single dose of the nosp-h*GLA* donor (1.2E+12 vg/mouse) and ZFN vectors (1.5E+11 vg/mouse each). A subset of the treated mice was administered daily oral doses of DGJ (3 mg/kg) starting at 30 days post-injection. *$p < 0.005$ when comparing ZFN and donor vector-treated Fabry mice administered DGJ versus those not administered DGJ. Fabry mice injected with only the nosp-*hGLA* donor and age- and sex-matched wild-type (WT) mice are included for comparison. Data presented are means ± SDs ($n \geq 5$).

whether or not the Kozak sequence or the T2A peptide were present, markedly increased their plasma α-Gal A activities during the 3 weeks post-injection and sustained activities that were 38-fold to 81-fold greater than mean wild-type levels for the entire 2-month study period (Figure 2B). Notably, Fabry mice treated with the *IDS*sp-h*GLA* donor achieved the highest plasma α-Gal A activities, which were continuously elevated ~250-fold greater than mean levels in wild-type mice (Figure 2B). Assessment of tissue α-Gal A activities at 2 months post-injection revealed that all three donors carrying the *GLAsp* led to similarly high enzyme expression, resulting in mean activities in the liver, heart, kidney, and spleen that were 11- to 24-fold, 6- to 9-fold, 0.6- to 1-fold, and 3- to 5-fold elevated, respectively, compared to mean wild-type levels (Figure 2C). Mice treated with the *IDS*sp-h*GLA* donor had even higher α-Gal A activities, averaging 73-, 25-, 2.4-, and 12-fold greater than mean wild-type levels in liver, heart, kidney, and spleen, respectively (Figure 2C).

In line with these findings, at 2 months post-injection, Fabry mice treated with the *GLA*sp-h*GLA*, Kozak-*GLA*sp-*h*GLA, and T2A-*GLA*sp-h*GLA* donors all had significant and similar reduction of Gb3 and Lyso-Gb3 in their plasma and tissues compared to formulation buffer-treated Fabry control mice (Figure 2D, data from T2A-*GLA*sp-h*GLA* donor group shown as representative treatment group). Mice that were administered the T2A-*GLA*sp-h*GLA* donor had liver Gb3 concentrations that were below the lower limit of quantitation (LLOQ) and ~1%, 7%, and 14% residual Gb3 in their plasma, heart, and kidney, respectively, relative to the formulation buffer-treated Fabry controls (Figure 2D). Lyso-Gb3 concentrations in the plasma, liver, heart, and kidney were markedly decreased to ~18%, 5%, 14%, and 14% of those in the controls, respectively (Figure 2D). Mice treated with the *IDS*sp-h*GLA* donor cleared substrates even more effectively, with no detectable Gb3 in plasma, liver, or heart and only ~7% remaining in the kidney. Lyso-Gb3 was completely cleared from heart, while plasma, liver, and kidney retained only ~6%, 2%, and 7% of controls, respectively, at 2 months post-injection (Figure 2D).

Vector genome copies for ZFN and donor constructs were assessed in all treatment groups, including the nosp-h*GLA* donor-treated mice (Figure 2E). There were no significant differences in ZFN or donor copy number between the groups, indicating that they all had similar rates of hepatocyte transduction. Donor vector genome copies were several-fold higher than ZFN vector genome copies due to the ratio of ZFNs to donor used in this study (i.e., one part left ZFN1 to one part right ZFN2 to eight parts h*GLA* donor). There were no significant differences in group mean indels, which ranged from 37.8% ± 6.2% for the nosp-h*GLA* group to 52.5% ± 12.3% for the T2A-*GLA*sp-h*GLA* group (data not shown).

To assess whether the liver-expressed α-Gal A enzyme was the mature form, western blot analysis was performed on liver extracts of Fabry mice treated with ZFN vectors and the *GLAsp*-h*GLA* or T2A-*GLA*sp-h*GLA* donor, using an anti-human α-Gal A antibody. As shown in Figure 3, the liver-expressed human α-Gal A enzyme was detected as a ~50 kDa band, consistent with our previous reports of the mature human α-Gal A enzyme,[34] while the human protein was not detected in untreated wild-type mouse livers. Digestion of the expressed enzyme with peptide N-glycosidase F (PNGase F) and endoglycosidase H (Endo H) yielded deglycoslyation patterns that were similar to those of Chinese hamster ovary (CHO)-cell-produced

Table 1. Quantification of indels in Fabry mice treated with ZFN vectors and/or the nosp-h*GLA* donor

Group	n	ZFN dose (vg/mouse)	Donor dose (vg/mouse)	Mean indels ± SD (%)
ZFNs + donor	7	1.50E+11	1.20E+12	45.2 ± 11.4
Donor only	4	0	1.20E+12	0.1 ± 0.1

vg, vector genomes.

recombinant human α-Gal A, indicating that the liver-expressed α-Gal A was appropriately glycosylated (Figure 3).

Thus, addition of a cleavable signal peptide to the nosp-h*GLA* donor markedly enhanced the hepatic production of mature, active α-Gal A enzyme that was appropriately glycosylated. The effective clearance of Gb3 and Lyso-Gb3 in key sites of pathology of Fabry mice indicated that the liver-produced enzyme was efficiently secreted into the circulation and subsequently taken up by target organs. Interestingly, substituting the *IDS* signal peptide sequence for the native *GLA* signal sequence resulted in markedly higher enzyme activity in plasma and tissues and the complete, or near-complete, clearance of the glycolipid substrates from key tissues.

AAV2/8-mediated delivery of ZFN vectors and the *IDS*sp-h*GLA* donor rapidly and effectively clears glycolipid substrates in Fabry mice, even at reduced doses

To evaluate AAV2/8 vector dose effect, Fabry mice were administered two different doses of the *IDS*sp-h*GLA* donor vector, 1.2E+12 vg/mouse (high dose; the same dose as used in Figure 2) or 4.0E+11 vg/mouse (low dose), along with proportionally adjusted doses of the ZFN vectors (5.0E+10 or 1.5E+10 vg/mouse per vector, respectively). To assess how rapidly the substrates are cleared, a subset of the treated mice was euthanized at 1 month, while the remaining mice were euthanized at 2 months, similar to the study above (Figures 2C and 2D).

Following co-administration of the *IDS*sp-h*GLA* donor and ZFN vectors, plasma α-Gal A activity markedly increased during the first 14 days post-injection and stabilized at levels that were ∼60- and 220-fold over wild-type levels for the low- and high-dose treatment groups, respectively (Figure 4A). At 2 months post-injection, the low-dose mice had mean tissue α-Gal A activities that were ∼12-, 10-, 1.7-, and 5-fold greater than mean wild-type levels in liver, heart, kidney, and spleen, respectively (Figure 4B). These levels were ∼4-fold lower in liver and ∼2-fold lower in heart, kidney, and spleen compared to the high-dose mice. Notably, tissue α-Gal A activities measured at 1 month post-injection were comparable to those at 2 months post-injection, regardless of the AAV dose administered (Figure 4B), suggesting that the uptake rate of circulating α-Gal A was constant over time and a function of enzyme concentration in the plasma. In line with these findings, the number of ZFN and donor vector genome copies in liver increased in a dose-dependent manner (Figure 4C). Additionally, ZFN and donor vector copy numbers were similar at 1 versus 2 months post-injection, in both the low- and high-dose treatment groups (Figure 4C).

As anticipated, at 2 months post-injection, the higher-dosed mice had essentially normal levels of Gb3 and Lyso-Gb3 in their plasma, liver, and heart, and only negligible Gb3 concentrations (5.3% ± 2.1% of untreated Fabry mice) in their kidneys (Figures 4D and 4E). Normalization of these substrates was achieved by 1-month post-injection (Figures 4D and 4E). Despite having reduced plasma and tissue α-Gal A activities, mice administered the low dose also had complete, or near-complete, substrate clearance in their plasma and tissues at both 1 and 2 months post-injection, with <7% of Lyso-Gb3 remaining in plasma and liver and ∼10% of Gb3 retained in kidney, compared to formulation buffer-treated Fabry control mice (Figures 4D and 4E). Gb3 and Lyso-Gb3 concentrations in heart were below the LLOQ, similar to wild-type mice.

These data indicate that the *IDS*sp-h*GLA* vector, even at a reduced dose, was highly effective in clearing accumulated glycosphingolipid substrates in key tissues. Importantly, both Gb-3 and Lyso-Gb3 were cleared relatively rapidly, by 4 weeks post-injection. The treatment was well-tolerated, even by the mice in the high-dose treatment group. Treated mice were clinically healthy and had normal or only slight elevation of liver transaminases when assessed at 2 months post-injection (Table 2). Mean plasma aspartate aminotransferase (AST) concentration in untreated Fabry mice was 65 ± 29 U/L, whereas in high-dose mice it was 89 ± 26 U/L, well within wild-type levels (99 ± 73 U/L). Mean plasma alanine aminotransferase (ALT) concentrations in untreated Fabry and wild-type mice were 12 ± 3 and 13 ± 3 U/L, respectively, while in the high-dose mice it was 33 ± 8 U/L. The high-dose mice had mean plasma albumin concentration of 2.4 ± 0.3 g/dL, comparable to those in untreated Fabry and wild-type control mice (2.7 ± 0.2 versus 2.2 ± 0.3, respectively; Table 2), indicating that this therapeutic approach did not disrupt normal production of albumin in the liver.

Donor integration in <10% of hepatocytes, mostly occurring via NHEJ, achieves complete or near-complete substrate clearance in key tissues

The *IDS*sp-h*GLA* donor construct was designed to include a next-generation sequencing (NGS) primer binding site and a targeted integration (TI) sequence for simultaneous quantification of indels and HDR-mediated integrations, respectively (Figure 5A, left panel; see also Materials and methods). When assessed 2 months post-injection, the frequency of indels in genomic DNA of livers ranged from 38.4% to 60.5% in Fabry mice treated with the *IDS*sp-h*GLA* donor and ZFN vectors (Figure 5A, right panel). There was no significant difference in the percent of indels between the low- and high-dose groups (44.6% ± 22.2% versus 47.7% ± 4.7%, respectively; means ± SDs). In contrast, control Fabry mice administered only the *IDS*sp-h*GLA* donor had <0.2% indels. Analysis of the donor-specific TI sequences demonstrated a dose-dependent increase in TI (Figure 5A, right panel), with the high-dose group having about twice as many HDR-integrated transgenes as the low-dose group (1.7% ± 0.4% versus 0.8% ± 0.2%, respectively, $p = 0.002$). No

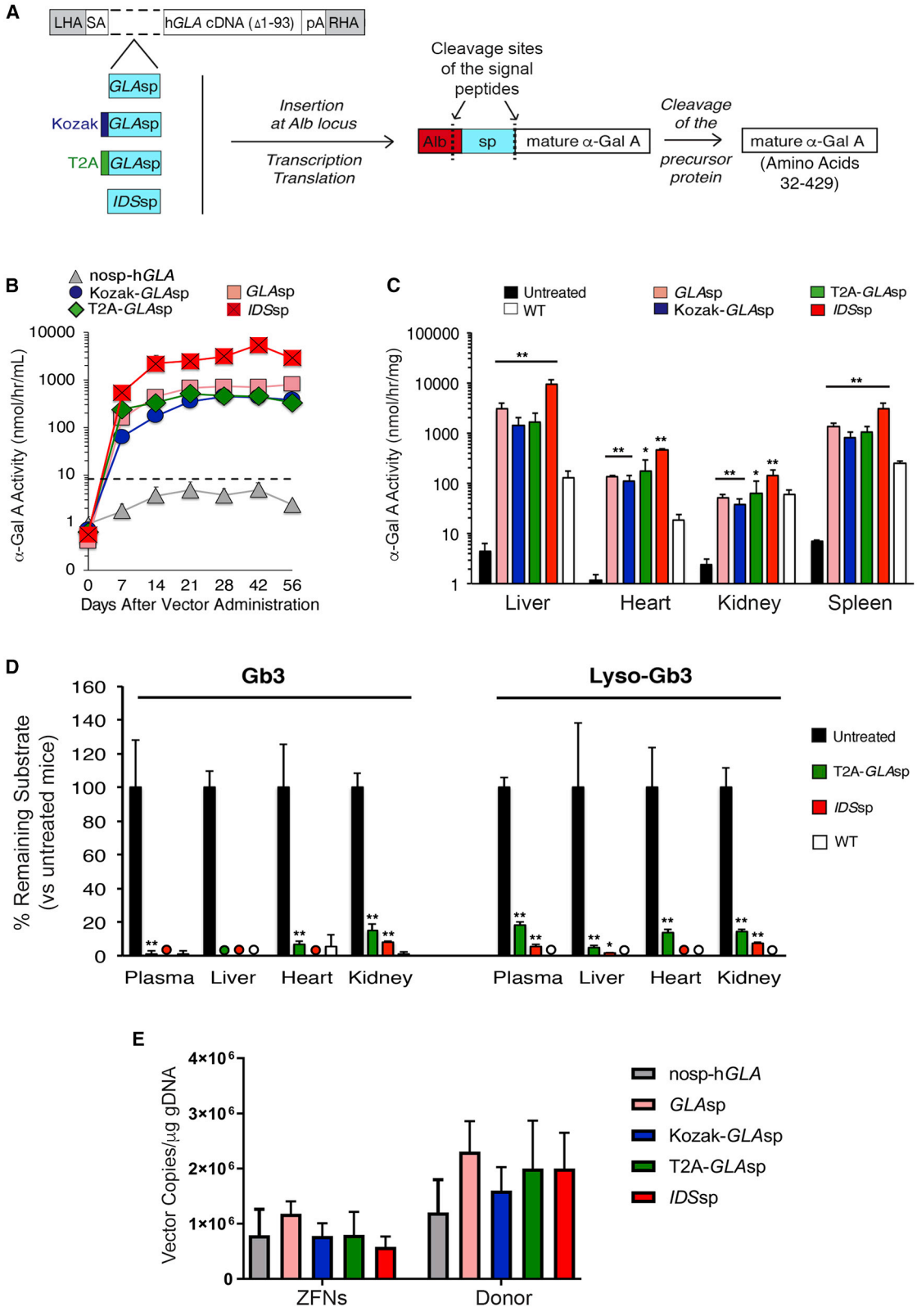

(legend on next page)

evidence of HDR-mediated integration was found in the donor-only or untreated Fabry mice.

While it was previously thought that ZFN-mediated targeted transgene insertion occurred primarily via HDR, recent studies have shown that NHEJ can also efficiently insert a therapeutic transgene into the ZFN-specified site.[35] The relatively low frequency of HDR-mediated integration events in this study suggested that the majority of donor integrations at the *Alb* locus occurred via the NHEJ pathway. This finding was confirmed by an *in-situ* hybridization assay using an RNA probe specific to the *Alb-IDS*sp-h*GLA* fusion transcript (Figure 5B, left panel). An estimated 5.6% and 9.8% of hepatocytes expressed the fusion transcript in the low- and high-dose groups, respectively (Figure 5B, right panel). Representative *in situ* hybridization images are shown in Figure 5C. By subtracting the average frequency of TI integration (i.e., HDR-mediated integration) from the percent of cells expressing the fusion transcript, the percentage of cells modified by NHEJ integration of the donor in the correct orientation for transgene expression was estimated to be 4.8% and 8.1% for the low- and high-dose treatment groups, respectively. Hepatocytes expressing the fusion transcript were not detected in mice treated with only the donor (Figures 5B, right panel, and 5C, left panel).

These results indicate that near-complete substrate reduction in the Fabry mice was achieved with less than 10% of hepatocytes being stably modified to express the human α-Gal A enzyme. Notably, the majority of donor integration occurred via NHEJ, rather than HDR.

DISCUSSION

Several characteristics of ZFNs make them particularly well-suited for therapeutic genome editing applications compared to the other programmable nucleases, including transcription activator-like effector nucleases (TALENs) and the clustered regularly interspaced short palindromic repeats (CRISPR)-CRISPR-associated protein 9 (Cas9) system. Modular ZFPs can be designed to recognize and bind extended targets up to 36 base pairs, which facilitates the high precision required for efficient and safe gene editing. This contrasts with the CRISPR-Cas9 system, which recognizes ~23 base pair DNA sequences, including the 2- to 5-nucleotide-long protospacer adjacent motif (PAM) sequence.[36,37] Recent studies have led to the development of improved design methods for the ZFP DNA-binding domain,[38,39] improved design of the FokI dimer interface[40,41] and cleavage domain,[39] and diversification of the ZFN architecture,[42] yielding highly specific ZFNs with little or no detectable off-target effects. Additionally, the compact size of ZFNs allows for efficient packaging into AAV vectors, which enables robust *in vivo* delivery, particularly to the liver. This is an advantage over TALENs, which are limited in their use of viral vector delivery platforms due to their relatively large size.[43]

Especially attractive is the AAV/ZFN-mediated *in vivo* protein replacement approach using *Alb* intron 1 as a safe harbor locus, which has recently been shown to be efficacious for the treatment of mouse disease models for hemophilia B[32] and mucopolysaccharidosis (MPS) type I and II.[30,31] A key advantage of this therapeutic platform is that transgene expression is driven by the highly active native *Alb* promoter, leading to constant high levels of transgene expression in stably modified hepatocytes. Diverting a small percentage of the transcriptional activity of the *Alb* promoter toward transgene expression should be clinically innocuous, as moderate decreases in albumin production are well tolerated.

We described here preclinical studies of AAV/ZFN-mediated *in vivo* protein replacement for Fabry disease by targeting the *Alb* safe harbor locus in α-Gal A-deficient Fabry mice. Integration of a signal-peptide-less h*GLA* transgene into the m*Alb* locus resulted in only modest increases of plasma and tissue α-Gal A activities, presumably due to misfolding of the enzyme in the endoplasmic reticulum (Figure 1C). This was contrary to previous studies in MPS I and II and hemophilia B mice, which achieved marked increases in expression of the therapeutic enzyme by integration of transgenes lacking their native signal peptide sequences.[30–32] Addition of a cleavable signal peptide (i.e., human *GLA* or *IDS* signal peptide) to the h*GLA* transgene resulted in continuous supraphysiological expression of α-Gal A activity, indicating that the protein misfolding in the absence of a signal peptide was due presumably to the two non-native amino acids that were retained on the N-terminus of the α-Gal A enzyme following cleavage of the albumin signal peptide (Figures 1A, 2B, and 2C). Interestingly, the *IDS* signal peptide achieved substantially higher levels of plasma and tissue α-Gal A activities compared to the native *GLA* signal peptide (Figures 2B and 2C). The superior performance of the *IDS*sp-h*GLA* donor was not due to increased transduction efficiency (Figure 2E). In fact, Fabry mice that were co-administered the *IDS*sp-h*GLA* donor and ZFN vectors, even at lower doses, had near-complete Gb3 and Lyso-Gb3 clearance in all

Figure 2. h*GLA* transgenes with signal peptides result in markedly increased α-Gal A activities and effective substrate clearance in Fabry mice

(A) Schematic representation of the four h*GLA* donors carrying cleavable signal peptides. Three of the constructs contained the h*GLA* signal peptide (*GLA*sp) at the 5′ end of the *GLA* cDNA, either by itself or preceded by a Kozak sequence or a 2A self-cleaving peptide (T2A), while the fourth contained the human iduronate 2-sulfatase signal peptide (*IDS*sp). Addition of a cleavable signal peptide right before the h*GLA* cDNA is expected to result in mature α-Gal A enzyme (amino acids 32–429) with no additional N-terminal amino acids carried over from the *Alb* signal peptide. (B) Time course of plasma α-Gal A activities following intravenous administration of ZFN vectors (1.5E+11 vg/mouse each) and one of the signal-peptide-containing *hGLA* donors (1.2E+12 vg/mouse) into male Fabry mice. The dotted line indicates mean α-Gal A activity in age-matched wild-type male mice. Data of Fabry mice treated with equivalent doses of the nosp-h*GLA* donor and ZFN vectors are shown for comparison. For all mouse groups treated with ZFN vectors and a signal-peptide-containing h*GLA* donor, $p < 0.001$ relative to wild type at 7 days post-injection and all time points thereafter. (C and D) Tissue α-Gal A activities (C) and percent (%) of Gb3 and Lyso-Gb3 remaining compared to formulation buffer-treated (untreated) male Fabry mice at 2 months post-injection (D) are shown. Data of untreated age-matched wild-type (WT) male mice are shown for comparison. In (C) and (D), $^{*}p < 0.05$ and $^{**}p < 0.005$ versus untreated Fabry mice. For (D), circles indicate that substrate concentrations were below the lower limit of quantitation. (E) Vector genome copies of the ZFN (ZFNs) and donor vectors (donor) quantitated in liver of treated male Fabry mice at 2 months post-injection, expressed as vector copies per μg of genomic DNA (gDNA). Note that the primers used to evaluate ZFN vector copy numbers do not distinguish between the left and right ZFNs. For (B)–(E), data presented are means ± SDs ($n \geq 3$).

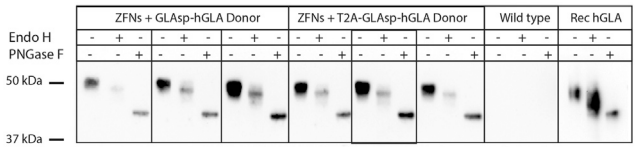

Figure 3. Liver-expressed α-Gal A enzyme is appropriately glycosylated

Livers isolated from three different male Fabry mice treated with ZFN vectors (1.5E+11 vg/mouse each) and the *GLA*sp-h*GLA* or T2A-*GLA*sp-h*GLA* donor (1.2E+12 vg/mouse) at 2 months post-injection were digested with Endo H or PNGase F, and the deglycosylated α-Gal A proteins were detected by western blot. An antibody raised specifically against human α-Gal A was used to avoid background signal from endogenous mouse α-Gal A in wild-type controls. Endo H cleaves the chitobiose core of high-mannose and some hybrid oligosaccharides from α-Gal A, resulting in a slightly smaller-sized protein. PNGase F cleaves the innermost *N*-acetylglucosamine and asparagine residues of high-mannose, hybrid, and complex oligosaccharides, thus removing nearly all *N*-linked oligosaccharides from the protein, leading to a much smaller protein. Representative images are shown for each treatment group. Wild-type mouse liver and Chinese hamster ovary (CHO)-cell-expressed recombinant human α-Gal A (rec hGLA), both undigested and glycosidase digested, were included as controls.

tissues examined, including heart and kidney (Figures 4D and 4E), with <10% of the hepatocytes expressing the *Alb-GLA* fusion mRNA (Figure 5B, right panel). The liver-expressed α-Gal A enzyme was appropriately glycosylated (Figure 3). Taken together, these results suggest that the liver-expressed enzyme was efficiently secreted into plasma and taken up by extra-hepatic tissues via M6P receptors.

It was notable that Fabry mice treated with *IDS*sp-h*GLA* donor only (at the equivalent dose of the high-dose group), in the absence of ZFN vectors, showed plasma α-Gal A activities comparable to those of wild-type mice (Figure 4A) and tissue activities that were considerably increased over baseline levels (Figure 4B). A similar phenomenon was observed in a mouse hepatocyte cell line, but not in a human hepatocyte cell line (data not shown), and was also reported in preclinical studies for *in vivo* genome editing in the MPS II mice.[30] Since there was no evidence of donor integration in these mice (Figure 5A, right panel), the modest activity from a promoter-less AAV construct was presumably due to inverted terminal repeat (ITR)-mediated transcription activation, as has been demonstrated by others.[44,45] Importantly, this seems to not occur in human cells, which rules out a therapeutic application. In addition, the level of plasma activity seen in the h*GLA* donor only group was >200-fold lower than mice treated with the equivalent donor dose in combination with ZFN vectors, highlighting the superior potency of integrating a transgene into the *Alb* locus via nucleases.

The frequency of HDR-mediated donor integration versus NHEJ-mediated integration was assessed in the treated Fabry mice. The majority of mature hepatocytes are in the G_0 phase of the cell cycle,[46] and therefore NHEJ is expected to be the predominant mechanism of double-stranded DNA repair.[47] Indeed, evidence from next-generation sequencing of genomic DNA and *in situ* hybridization of mRNA from liver of treated Fabry mice (Figures 5A, right panel and 5B, right panel) indicated that NHEJ-mediated integrations were ~5- to 6-fold more frequent than HDR-mediated integrations. The added SA site 5′ of the h*GLA* cDNA should lead to expression of the *Alb-GLA* hybrid mRNA regardless of the whether the h*GLA* donor sequence was integrated via HDR or NHEJ, as long as the NHEJ-mediated insertion of the donor occurred in the correct orientation. On the contrary, integration of the donor in the opposite orientation results in the entire donor sequence being removed during mRNA splicing.

One concern regarding NHEJ-mediated integration events is the potential for the partial or full-length ITR sequence to be inserted along with the donor transgene. The AAV ITRs have the potential to activate transcription, as has been observed in our studies and by others.[44,45] Insertion of ITRs from recombinant AAV has been implicated in clonal expansion of hepatocytes in a dog model of hemophilia[48] and linked to the development of hepatocarcinoma in mice,[49–51] but not in non-human primates.[52] To date, no evidence of clonal expansion or hepatocarcinoma has been detected in patients treated with recombinant AAV vectors, suggesting that the risk of recombinant AAV-vector-integration-derived oncogenesis in liver is very low in humans.

A major advantage of *in vivo* genome editing over ERT—the current standard of care treatment for Fabry disease—is that it offers the potential for a one-time treatment as opposed to lifelong biweekly 2- to 4-h infusions. The fact that it delivers a constant supply of therapeutic enzyme rather than the peak-and-trough levels of recombinant α-Gal A activity provided by ERT may also be advantageous, as the genome-editing therapy cleared the accumulated substrates from the targeted tissues, particularly from the kidney, more effectively than did eight recombinant α-Gal A infusions (administered every other day) into the Fabry mice.[29] Unlike chaperone therapy, which is not effective for all *GLA* mutations,[20–22] the *in vivo* genome editing approach is applicable to patients with type 1 or type 2 disease. While the efficacy of AAV-mediated liver-directed gene therapy approaches has been previously demonstrated in the Fabry mice by us and others,[53–56] the genome-editing strategy described here leads to the permanent integration of the h*GLA* transgene and therefore permits treatment of children and/or adolescents with Fabry disease whose liver cells are still dividing as the liver grows. This is of significant importance, as it is well established that treatments for Fabry disease are more effective if initiated early, particularly before irreversible organ damage occurs.[2,13,15–17] Newborn screening for Fabry disease, which is already implemented in Taiwan and several states in the United States, will facilitate early diagnosis and therapeutic intervention in the future.

In summary, ZFN-mediated *in vivo* genome editing in Fabry mouse liver led to continuous supraphysiologic levels of plasma and tissue α-Gal A activities, resulting in complete or near-complete clearance of the accumulated glycolipid substrates in key sites of organ pathology and dysfunction. These studies provide further preclinical evidence for this ZFN-mediated *in vivo* genome editing approach. Clinical trials for other lysosomal storage disorders using this approach produced evidence of genome editing with transiently increased enzyme activity,[57,58] despite achieving stable therapeutic levels of circulating enzyme in mouse models,[30,31] underlining the translational challenges associated with *in vivo* genome editing. Recent efforts have been directed

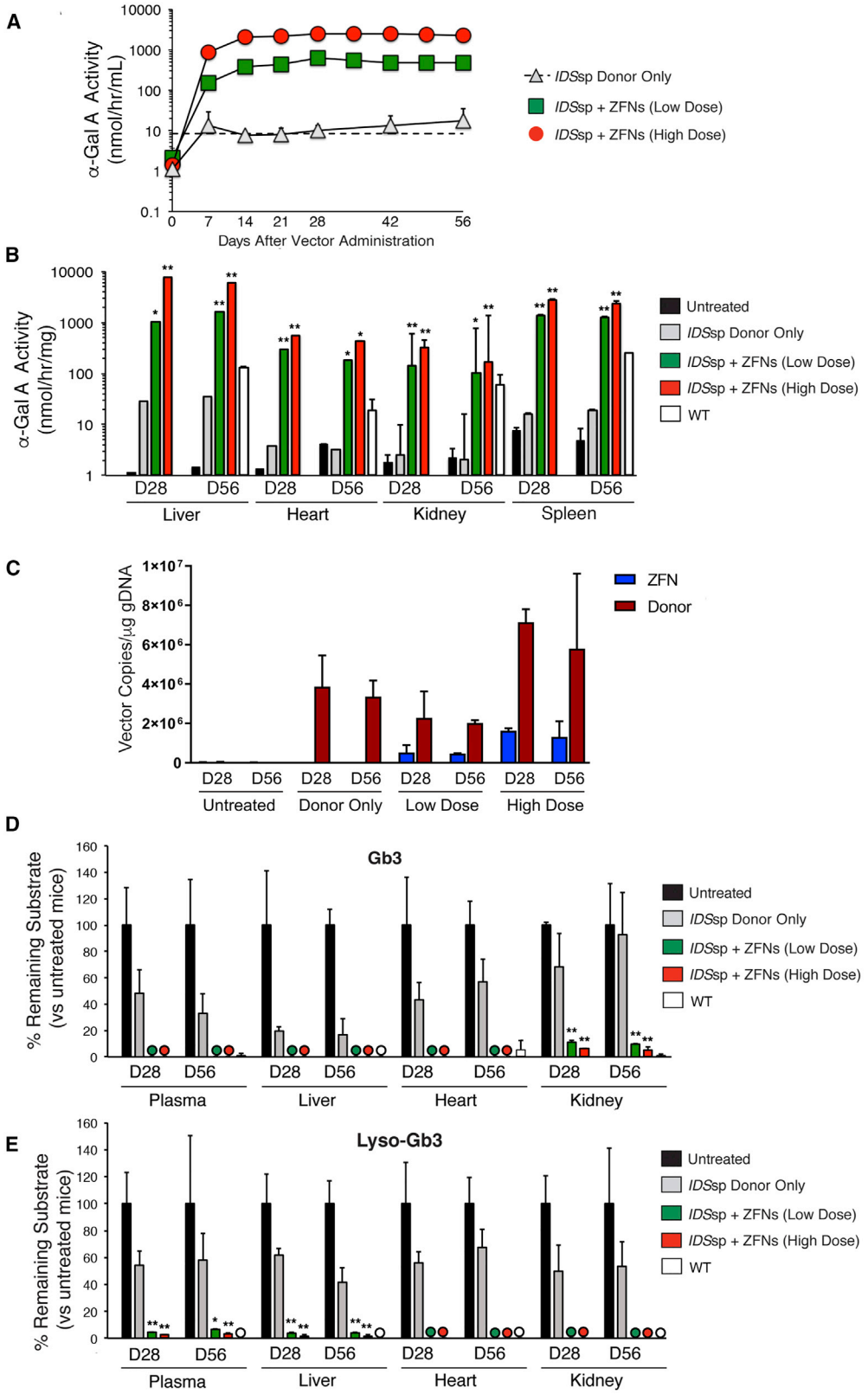

(legend on next page)

Table 2. Liver transaminase and albumin levels are essentially normal in high-dose-treated Fabry mice

	WT	Fabry untreated	Fabry high-dose treated
AST (U/L)	98.7 ± 73.1	64.7 ± 28.5	89.3 ± 25.8
ALT (U/L)	13.3 ± 2.5	12.3 ± 3.1	32.7 ± 7.6
Albumin (g/dL)	2.2 ± 0.3	2.7 ± 0.2	2.4 ± 0.3

Plasma samples were assessed for liver transaminase and albumin concentrations in wild-type male mice (WT), untreated Fabry mice, and Fabry mice administered a single high dose of the *IDS*sp-h*GLA* donor (1.2E+12 vg/mouse) and the ZFN vectors (5E+10 vg/mouse per vector), 2 months post-treatment. Values shown are means ± SDs (n = 3). AST, aspartate transaminase; ALT, alanine transaminase.

to developing an improved ZFN platform for efficacious, high-precision genome editing and have resulted in several new strategies that significantly increased the degree of precision, efficacy, and specificity of the therapeutic ZFNs.[39,42] These strategies are currently undergoing further preclinical evaluation. An AAV-mediated liver-directed gene therapy approach for treating Fabry disease was developed in tandem with the ZFN genome-editing strategy and was able to achieve even higher levels of plasma and tissue α-Gal A activity in mice.[54] This gene therapy approach is currently being evaluated in a phase I/II clinical trial (see https://clinicaltrials.gov/ct2/show/NCT04046224) to address the urgent need for new, long-lasting therapies for Fabry disease.

MATERIALS AND METHODS

Generation and packaging of ZFNs and h*GLA* donor constructs into AAV2/8

Heterodimeric ZFNs targeting intron 1 of the murine or human (i.e., for HepG2 cell studies) albumin locus were generated as previously described,[32,35] with the obligate heterodimer ELD/KKR mutations in the *FokI* domain.[40] To improve transgene expression, driven by the human alpha 1-antitrypsin promoter, a woodchuck hepatitis virus post-transcriptional regulatory element (WPRE) sequence was added to the 3′ untranslated region of the ZFNs.[59] The h*GLA* donor construct contained a codon-optimized h*GLA* cDNA encoding amino acids 32–429 of the mature enzyme, preceded by the endogenous h*GLA* signal peptide (amino acids 1–31), the *IDS* signal peptide, or no signal peptide. All h*GLA* donor constructs contained a human factor IX SA sequence and arms of homology to the mouse or human albumin target site (Figure 1A). Recombinant AAV2/8 vectors, comprising AAV2 ITRs and the AAV8 capsid, were produced by triple transfection of human embryonic kidney (HEK) 293 cells in 10-chamber Corning CELLSTACK culture chambers (Corning, NY, USA) and purified by cesium chloride density gradient centrifugation and dialysis. AAV vectors were titered as previously described.[60,61]

In vitro transduction of HepG2 cells and single-cell subcloning by limiting dilution

HepG2/C3A cells (ATCC, Manassas, VA, USA; CRL-10741) were maintained in Minimum Essential Medium (MEM; Corning) with 10% fetal bovine serum (FBS; Life Technologies, Carlsbad, CA, USA) and 1× penicillin-streptomycin-glutamine (Life Technologies) and incubated at 37°C with 5% CO_2. For transduction, cells were rinsed and trypsinized with 0.25% trypsin/2.2 mM ethylenediaminetetraacetic acid (EDTA) (Corning) and re-suspended in growth media. A small aliquot was mixed 1:1 with trypan blue solution 0.4% (w/v) in phosphate-buffered saline (PBS; Corning), and cells were counted on the TC20 Automated Cell Counter (Bio-Rad, Hercules, CA, USA). Cells were seeded into Corning 24-well plates (1.0E+05 viable cells in 0.5 mL media per well) and recombinant AAV2/8 particles containing the h*GLA* donor and heterodimeric ZFNs, diluted in growth medium, were added. The multiplicity of infection (MOI) was 3.0E+05 vg/cell for each ZFN and 6.0+05 vg/cell for the h*GLA* donor, representing a ZFN1:ZFN2:donor ratio of 1:1:2, which was previously determined to be optimal for *in vitro* transductions.[44]

On day 7 post-transduction, cells were washed, trypsinized, and re-suspended in growth media at densities of 10, 30, and 50 cells/mL and then plated into Corning 96-well culture plates at 100 μL per well. After 2 weeks, the wells containing single colonies were trypsinized and re-seeded into 24-well plates. Two days later, the growth media supernatants were harvested, flash-frozen on dry ice, and assessed for α-Gal A activities, as described below. Clones secreting high levels of α-Gal A were plated into 6-well plates and incubated with 0, 2, or 20 μM of DGJ (Sigma Aldrich, St. Louis, MO, USA) for 24 h. Cells were harvested, lysed in lysosomal buffer (0.1 M citrate/0.2 M phosphate buffer [pH 4.6] containing 1% Triton X-100), and intracellular α-Gal A activities were determined. Clonality was verified via next-generation sequencing.

Preclinical studies in the Fabry mouse model

Fabry mice were previously generated via homologous recombination in 129/Sv embryonic stem cells.[29,62] Once colonies were established, the mice were backcrossed onto the C57BL/6J background and maintained in a barrier facility at the Icahn School of Medicine at Mount Sinai (ISMMS). All animal procedures were reviewed and approved

Figure 4. The *IDS*sp-h*GLA* donor effectively and rapidly clears substrates, even at lower vector doses

Male Fabry mice were administered a high (1.2E+12 vg/mouse) or low dose (4.0E+11 vg/mouse) of the *IDS*sp-h*GLA* donor and the ZFN vectors (1.5E+11 or 5E+10 vg/mouse per vector, respectively). (A and B) Plasma (A) and tissue (B) α-Gal A activities, determined at the indicated days post-injection, are presented as means ± SDs (n ≥ 3). Dotted line shows mean activity in untreated age-matched wild-type male mice. In (A), $p < 0.001$ for low- and high-dosed mice versus untreated Fabry mice on day 7 and all time points after, whereas for (B), *$p < 0.05$ and **$p < 0.005$ versus untreated Fabry mice. (C–E) ZFN or donor-vector genome copy numbers per μg of genomic DNA (gDNA) in the liver (C) and the percentage of residual Gb3 (D) and Lyso-Gb3 (E) compared to formulation buffer-treated (untreated) male Fabry mice at days 28 and 56 post-injection are presented as means ± SDs (n ≥ 3, with the exception of the low-dose D28 and D56 groups, for which n = 2). Data of male Fabry mice administered the *IDS*sp-h*GLA* donor (1.2E+12 vg/mouse) without the ZFN vectors (donor only), as well as wild-type (WT) males, are also shown. Circles indicate that substrate concentrations were below the lower limit of quantitation. In (D) and (E), *$p < 0.05$ and **$p < 0.01$ versus untreated Fabry mice.

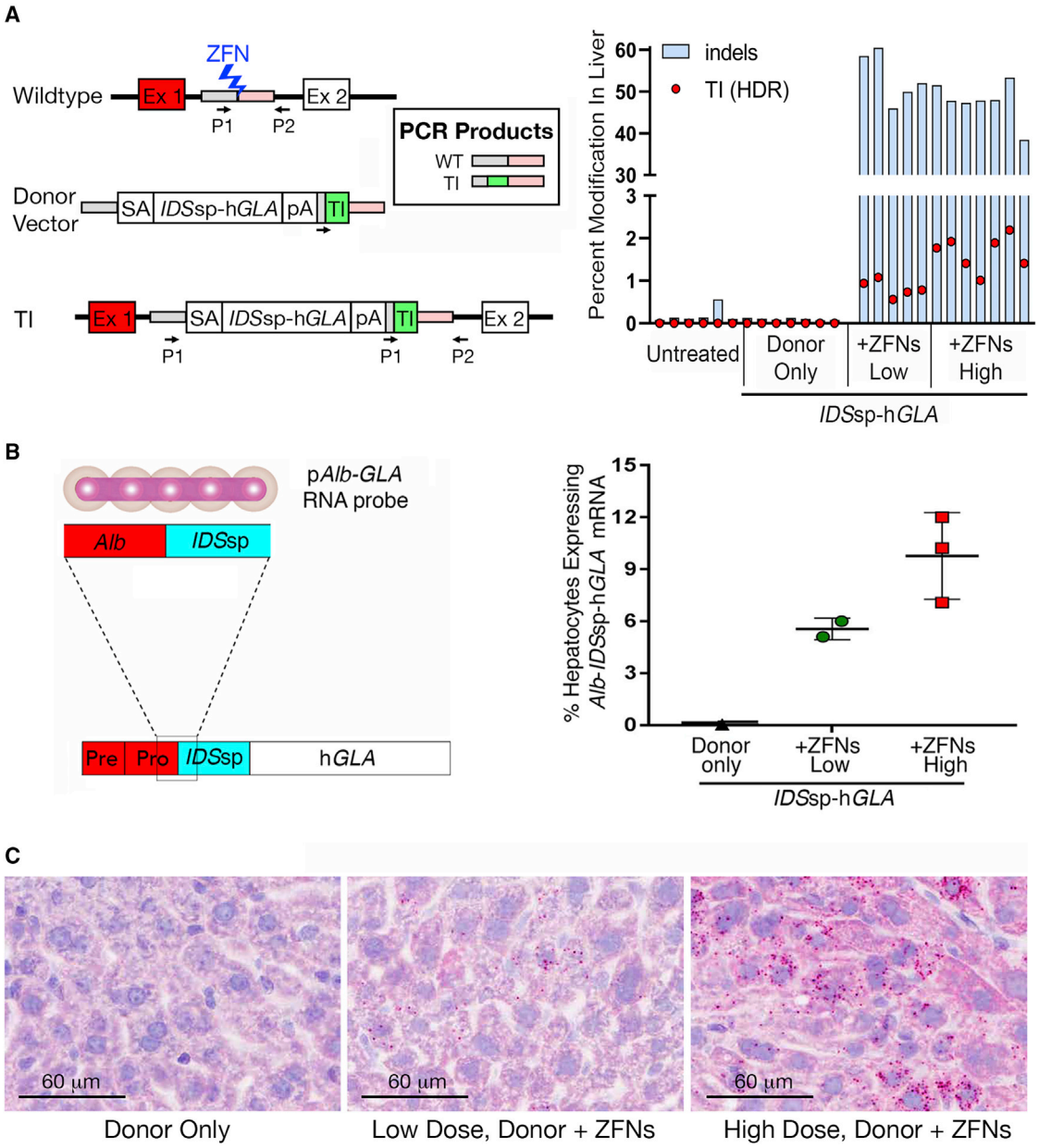

Figure 5. Stable integration of h*GLA* cDNA in less than 10% of hepatocytes essentially normalizes substrates in Fabry mice

(A) Left panel, the wild-type (WT) murine albumin (m*Alb*) locus is depicted with the left and right homology arms shown in gray and pink boxes, respectively. Exon 1 (Ex 1), which contains the albumin secretory signal peptide, is shown in red. Next-generation sequencing primer P1 was designed to recognize a sequence within the left homology arm, while primer P2 recognized a sequence immediately outside of the right homology arm. The *IDS*sp-h*GLA* donor contained a P1 binding site, followed by a unique 50-nucleotide targeted integration (TI) sequence, to simultaneously detect indels and HDR-meditated integration events following PCR amplification. Right panel, quantification of the percentage of liver cells containing indels and TI sequences in male Fabry mice treated with the low (4E+11 vg/mouse) or high (1.2E+12 vg/mouse) doses of the *IDS*sp-h*GLA* donor and ZFN vectors (1.5E+10 or 5.0E+10 vg/mouse per vector, respectively), relative to those treated with only the high-dose donor vector (donor only) or untreated controls. Individual mice are represented by a blue column, showing indels, overlaid with a red circle, displaying HDR integration events. Statistical analyses comparing TI integrations for the low- versus high-dose groups showed p = 0.002. (B) Left panel, an RNA probe (p*Alb-GLA* probe) that specifically recognizes the m*Alb*-h*GLA* fusion junction site was used to quantitate the percentage of hepatocytes expressing the m*Alb*-h*GLA* fusion transcript by *in situ* hybridization, as shown in the right panel. Each square, circle, and triangle represents data of an individual mouse, whereas bold horizontal lines indicate mean values and non-bold lines represent SDs (n = 2, 2, and 3 for the donor-only control, low dose, and high dose, respectively). (C) Representative *in situ* hybridization images of livers isolated from male Fabry mice treated with high-dose *IDS*sp-h*GLA* donor only (left panel) and low and high doses of the ZFN and donor vectors (middle and right panels, respectively). Positive hybridization signals are identified as red, punctate dots when visualized under bright-field microscopy. Samples were counterstained with Gill's hematoxylin and are shown at 40× magnification.

by the ISMMS Internal Animal Care and Use Committee (IACUC). Only male mice were used for these studies. AAV2/8 vectors formulated in 200 μL of PBS and 0.001% Pluronic F68 were injected into the tail veins of 8- to 12-week-old Fabry males, at the indicated doses (ZFN1:ZFN2:donor ratio of 1:1:8). Mice were immunosuppressed once every 2 weeks with intraperitoneal injections of cyclophosphamide (50 mg/kg) starting the day before vector administration. DGJ (3 mg/kg/day) was administered daily by oral gavage. Blood samples were collected in EDTA K2-coated tubes from facial veins, and plasma was isolated by centrifugation at 2,500 × *g* for 10 min. Mice were sacrificed at the indicated time points by perfusion with PBS via the left ventricle under ketamine/xylazine anesthesia, and tissues were snap-frozen in liquid nitrogen and stored at −80°C until use.

α-Gal A enzymatic activity assays

Tissue samples were homogenized in chilled reporter lysis buffer (Promega, Madison, WI, USA), and protein concentrations were determined using the Bio-Rad Bradford Protein Assay. α-Gal A activity was determined using a fluorometric assay, as previously described.[63] Briefly, 10 μL of HepG2 cell lysate or murine plasma or tissue lysate was incubated with an equal volume (10 μL) of 10 mM 4-methylumbelliferyl-α-D-galactopyranoside (Sigma-Aldrich), dissolved in assay buffer (0.2 M citrate, 0.4 M phosphate buffer [pH 4.4]), and 0.1 M N-acetylgalactosamine (Amersham Pharmacia Biotech, Little Chalfont, UK), the latter to inhibit α-galactosidase B activity.[64] Following incubation for 30 min at 37°C, reactions were terminated by the addition of 0.1 M ethylenediamine (pH 10.3, 480 μL). The amount of 4-methylumbelliferone (4-MU) produced was determined by measuring fluorescence using a Modulus fluorometer (Turner Biosystems, Sunnyvale, CA, USA). Plasma α-Gal A activities were expressed as nanomoles of 4-MU produced per hour per mL (nmol/h/mL), while tissue or HepG2 intracellular α-Gal A activity was expressed as nmol of 4-MU produced per hour per mg of total protein (nmol/h/mg).

DNA purification and vector genome quantitation

Total DNA was isolated from liver, and ZFN and h*GLA* donor vector copy numbers were determined using previously described methods.[54] ZFN vector copy numbers were detected using forward primer 5′-GTGGAGGAGCTGCTGATCG-3′, reverse primer 5′-GAAGTTGATCTCGCCGTTGTTGA-3′ and probe 5′- ATGATCAAAGCCGGCACCCTGACA-3′. These primers were designed to anneal to a sequence present in both the left and right ZFNs. h*GLA* donor copy numbers were detected using forward primer 5′-GCGGAGTTCCAATTGTACTGT-3′, reverse primer 5′-TCCTAAGTGCACCCACTGAT-3′ and probe 5′-AACGCTAGCGTGCCGACCTG-3′. Data were processed using QuantStudio Design and Analysis software and expressed as vg copies per μg gDNA.

Gb3 and Lyso-Gb3 analyses in plasma and tissue samples

Gb3 and Lyso-Gb3 concentrations were determined in tissues and plasma using liquid chromatography-mass spectrometry (LC-MS) at Brains-Online (Charles River Laboratories, Wilmington, MA, USA), as previously described.[54] LLOQs were as follows: Lyso-Gb3 = 1 nM for plasma, 0.05 nmol/g for heart and liver, and 0.1 nmol/g for kidney; Gb3 = 60 nM for plasma, 3 nmol/g for heart and liver, and 6 nmol/g for kidney.

Simultaneous indel and TI detection by next-generation sequencing

Genomic DNA was isolated from livers, and a DNA fragment flanking the *Alb* intron 1 ZFN target site was amplified by polymerase chain reaction (PCR) using P1 and P2 primers (Figure 5A, left panel; P1 = forward primer, 5′-ACACGACGCTCTTCCGATCTNNNNTTGAGTTTGAATGCACAGAT-3′; P2 = reverse primer, 5′-GACGTGTGCTCTTCCGATCTNNNNGAAACAGGGAGAGAAAAACC-3′). Paired-end deep sequencing was performed on the MiSeq system (Illumina, San Diego, CA, USA), and SeqPrep software (https://github.com/jstjohn/SeqPrep) was used to trim adapters and merge the paired reads. The Needleman-Wunsch algorithm was used to align merged reads to the wild-type sequence and map the insertions and deletions and to distinguish the TI sequence incorporated into the *IDS*sp-h*GLA* donor. The TI sequence consists of a 50 bp segment of murine albumin intron 1 that has been randomly scrambled to produce a unique amplicon for the detection of alleles in which the *IDS*sp-h*GLA* donor was integrated. The TI sequence is immediately preceded by a P1 primer binding site (Figure 5A, left panel) to ensure that wild-type and TI integration-derived amplicons are the same length. ZFN activity is reported as % indels, the fraction of sequenced amplicons that differ from wild-type due to insertions or deletions.

In situ hybridization assay to detect the *Alb*-h*GLA* fusion transcript

Formalin-fixed paraffin-embedded (FFPE) liver tissues were sliced into 5 μm sections. RNA *in situ* hybridization was performed manually using the BaseScope Red Reagent Kit (Advanced Cell Diagnostics, Newark, CA, USA), according to the manufacturer's instructions and an RNA probe (p*Alb-GLA*; Figure 5B, left panel) that specifically detects the fusion junction of the *Alb*-h*GLA* transcript. Briefly, FFPE liver sections were pretreated with heat and protease and hybridized sequentially with pre-preamplifier, preamplifier, amplifier, and then the alkaline phosphatase (AP)-labeled target oligo, followed by chromogenic precipitate development. Each sample was quality controlled for RNA integrity using a BaseScope probe specific to peptidyl-prolyl cis-trans isomerase B (*Ppib*) RNA, while a probe specific to bacterial dihydrodipicolinate reductase (dapB) RNA confirmed low off-target signal levels. Specific RNA-staining signals were identified as red, punctate dots. Samples were counterstained with Gill's hematoxylin, and bright-field images were acquired using an AperioAT2 digital slide scanner equipped with a 40× objective. The percentage of hepatocytes positive for the p*Alb-GLA* probe was determined using the HALO quantification software (Indica Labs, Albuquerque, NM, USA).

Western blot analysis to assess glycosylation profile of liver-expressed α-Gal A

Frozen liver tissue (~50 mg) was processed, digested with Endo H or PNGase F (both from New England Biolabs, Ipswich, MA, USA), and analyzed by western blot as previously described[54] to assess the glycosylation pattern of the liver-expressed α-Gal A enzyme.

Statistical analyses

Statistical analyses were performed using unpaired one-tailed Student's t test. Differences of $p < 0.05$ were considered statistically significant.

ACKNOWLEDGMENTS

This work was funded by a research grant from Sangamo Therapeutics, Inc. The authors are grateful to Lisa King, Carolyn Gasper, and Daniel Richards for their contributions to designing and overseeing the conduct of the animal studies and sample analysis.

AUTHOR CONTRIBUTIONS

Conceptualization, M.W.H., M.C.H., and T.W.; methodology, S.P., M.W.H., T.W., R.J.D., and M.Y.; investigation, S.P., M.W.H., L.M., L.G., S.S.M., S.S., and M.Y.; writing, S.P., M.W.H., and M.Y.; supervision, M.D.H., K.M., T.W., R.J.D., and M.Y.

DECLARATION OF INTERESTS

R.J.D. is a consultant to Genzyme-Sanofi and Sangamo Therapeutics, Inc. He owns founder stock in Amicus Therapeutics and options for Sangamo Therapeutics, Inc. and receives royalties from Genzyme-Sanofi. R.J.D. and M.Y. received a research grant from Sangamo Therapeutics, Inc. to perform these studies. M.W.H., S.S.M., S.S., K.M., M.C.H., and T.W. are full-time employees and/or shareholders of Sangamo Therapeutics, Inc.

REFERENCES

1. Desnick, R.J., Ioannou, Y.A., and Eng, C.M. (2001). α-galactosidase A deficiency: Fabry disease. In The Metabolic and Molecular Bases of Inherited Disease, C.R. Scriver, A.L. Beaudet, W.S. Sly, D. Valle, K.E. Kinzler, and B. Volgelstein, eds. (McGraw-Hill), pp. 3733–3774.
2. Aerts, J.M., Groener, J.E., Kuiper, S., Donker-Koopman, W.E., Strijland, A., Ottenhoff, R., van Roomen, C., Mirzaian, M., Wijburg, F.A., Linthorst, G.E., et al. (2008). Elevated globotriaosylsphingosine is a hallmark of Fabry disease. Proc. Natl. Acad. Sci. USA *105*, 2812–2817.
3. Elleder, M. (2008). Cellular and tissue localization of globotriaosylceramide in Fabry disease. Virchows Arch. *452*, 705, author reply 707–708.
4. Thurberg, B.L., Fallon, J.T., Mitchell, R., Aretz, T., Gordon, R.E., and O'Callaghan, M.W. (2009). Cardiac microvascular pathology in Fabry disease: evaluation of endomyocardial biopsies before and after enzyme replacement therapy. Circulation *119*, 2561–2567.
5. Thurberg, B.L., Rennke, H., Colvin, R.B., Dikman, S., Gordon, R.E., Collins, A.B., Desnick, R.J., and O'Callaghan, M. (2002). Globotriaosylceramide accumulation in the Fabry kidney is cleared from multiple cell types after enzyme replacement therapy. Kidney Int. *62*, 1933–1946.
6. Desnick, R.J., and Banikazemi, M. (2006). Fabry disease: clinical spectrum and evidence-based enzyme replacement therapy. Nephrol. Ther. *2* (*Suppl 2*), S172–S185.
7. Desnick, R.J., and Wasserstein, M.P. (2001). Fabry disease: clinical features and recent advances in enzyme replacement therapy. Adv. Nephrol. Necker Hosp. *31*, 317–339.
8. Nakao, S., Kodama, C., Takenaka, T., Tanaka, A., Yasumoto, Y., Yoshida, A., Kanzaki, T., Enriquez, A.L., Eng, C.M., Tanaka, H., et al. (2003). Fabry disease: detection of undiagnosed hemodialysis patients and identification of a "renal variant" phenotype. Kidney Int. *64*, 801–807.
9. von Scheidt, W., Eng, C.M., Fitzmaurice, T.F., Erdmann, E., Hübner, G., Olsen, E.G., Christomanou, H., Kandolf, R., Bishop, D.F., and Desnick, R.J. (1991). An atypical variant of Fabry's disease with manifestations confined to the myocardium. N. Engl. J. Med. *324*, 395–399.
10. Nakao, S., Takenaka, T., Maeda, M., Kodama, C., Tanaka, A., Tahara, M., Yoshida, A., Kuriyama, M., Hayashibe, H., Sakuraba, H., et al. (1995). An atypical variant of Fabry's disease in men with left ventricular hypertrophy. N. Engl. J. Med. *333*, 288–293.
11. Echevarria, L., Benistan, K., Toussaint, A., Dubourg, O., Hagege, A.A., Eladari, D., Jabbour, F., Beldjord, C., De Mazancourt, P., and Germain, D.P. (2016). X-chromosome inactivation in female patients with Fabry disease. Clin. Genet. *89*, 44–54.
12. Eng, C.M., Banikazemi, M., Gordon, R.E., Goldman, M., Phelps, R., Kim, L., Gass, A., Winston, J., Dikman, S., Fallon, J.T., et al. (2001). A phase 1/2 clinical trial of enzyme replacement in fabry disease: pharmacokinetic, substrate clearance, and safety studies. Am. J. Hum. Genet. *68*, 711–722.
13. Eng, C.M., Guffon, N., Wilcox, W.R., Germain, D.P., Lee, P., Waldek, S., Caplan, L., Linthorst, G.E., and Desnick, R.J.; International Collaborative Fabry Disease Study Group (2001). Safety and efficacy of recombinant human alpha-galactosidase A replacement therapy in Fabry's disease. N. Engl. J. Med. *345*, 9–16.
14. Germain, D.P., Charrow, J., Desnick, R.J., Guffon, N., Kempf, J., Lachmann, R.H., Lemay, R., Linthorst, G.E., Packman, S., Scott, C.R., et al. (2015). Ten-year outcome of enzyme replacement therapy with agalsidase beta in patients with Fabry disease. J. Med. Genet. *52*, 353–358.
15. Desnick, R.J., Brady, R., Barranger, J., Collins, A.J., Germain, D.P., Goldman, M., Grabowski, G., Packman, S., and Wilcox, W.R. (2003). Fabry disease, an under-recognized multisystemic disorder: expert recommendations for diagnosis, management, and enzyme replacement therapy. Ann. Intern. Med. *138*, 338–346.
16. Germain, D.P., Elliott, P.M., Falissard, B., Fomin, V.V., Hilz, M.J., Jovanovic, A., Kantola, I., Linhart, A., Mignani, R., Namdar, M., et al. (2019). The effect of enzyme replacement therapy on clinical outcomes in male patients with Fabry disease: A systematic literature review by a European panel of experts. Mol. Genet. Metab. Rep. *19*, 100454.
17. Ortiz, A., Germain, D.P., Desnick, R.J., Politei, J., Mauer, M., Burlina, A., Eng, C., Hopkin, R.J., Laney, D., Linhart, A., et al. (2018). Fabry disease revisited: Management and treatment recommendations for adult patients. Mol. Genet. Metab. *123*, 416–427.
18. Lenders, M., Stypmann, J., Duning, T., Schmitz, B., Brand, S.M., and Brand, E. (2016). Serum-Mediated Inhibition of Enzyme Replacement Therapy in Fabry Disease. J. Am. Soc. Nephrol. *27*, 256–264.
19. Linthorst, G.E., Hollak, C.E., Donker-Koopman, W.E., Strijland, A., and Aerts, J.M. (2004). Enzyme therapy for Fabry disease: neutralizing antibodies toward agalsidase alpha and beta. Kidney Int. *66*, 1589–1595.
20. Benjamin, E.R., Della Valle, M.C., Wu, X., Katz, E., Pruthi, F., Bond, S., Bronfin, B., Williams, H., Yu, J., Bichet, D.G., et al. (2017). The validation of pharmacogenetics for the identification of Fabry patients to be treated with migalastat. Genet. Med. *19*, 430–438.
21. Lukas, J., Giese, A.K., Markoff, A., Grittner, U., Kolodny, E., Mascher, H., Lackner, K.J., Meyer, W., Wree, P., Saviouk, V., and Rolfs, A. (2013). Functional characterisation of alpha-galactosidase a mutations as a basis for a new classification system in fabry disease. PLoS Genet. *9*, e1003632.
22. Wu, X., Katz, E., Della Valle, M.C., Mascioli, K., Flanagan, J.J., Castelli, J.P., Schiffmann, R., Boudes, P., Lockhart, D.J., Valenzano, K.J., and Benjamin, E.R. (2011). A pharmacogenetic approach to identify mutant forms of α-galactosidase A that respond to a pharmacological chaperone for Fabry disease. Hum. Mutat. *32*, 965–977.
23. Bolukbasi, M.F., Liu, P., Luk, K., Kwok, S.F., Gupta, A., Amrani, N., Sontheimer, E.J., Zhu, L.J., and Wolfe, S.A. (2018). Orthogonal Cas9-Cas9 chimeras provide a versatile platform for genome editing. Nat. Commun. *9*, 4856.
24. Ceccaldi, R., Rondinelli, B., and D'Andrea, A.D. (2016). Repair Pathway Choices and Consequences at the Double-Strand Break. Trends Cell Biol. *26*, 52–64.
25. Chapman, J.R., Taylor, M.R., and Boulton, S.J. (2012). Playing the end game: DNA double-strand break repair pathway choice. Mol. Cell *47*, 497–510.
26. Bibikova, M., Beumer, K., Trautman, J.K., and Carroll, D. (2003). Enhancing gene targeting with designed zinc finger nucleases. Science *300*, 764.
27. Kim, Y.G., Cha, J., and Chandrasegaran, S. (1996). Hybrid restriction enzymes: zinc finger fusions to Fok I cleavage domain. Proc. Natl. Acad. Sci. USA *93*, 1156–1160.

28. Smith, J., Bibikova, M., Whitby, F.G., Reddy, A.R., Chandrasegaran, S., and Carroll, D. (2000). Requirements for double-strand cleavage by chimeric restriction enzymes with zinc finger DNA-recognition domains. Nucleic Acids Res. *28*, 3361–3369.

29. Ioannou, Y.A., Zeidner, K.M., Gordon, R.E., and Desnick, R.J. (2001). Fabry disease: preclinical studies demonstrate the effectiveness of alpha-galactosidase A replacement in enzyme-deficient mice. Am. J. Hum. Genet. *68*, 14–25.

30. Laoharawee, K., DeKelver, R.C., Podetz-Pedersen, K.M., Rohde, M., Sproul, S., Nguyen, H.O., Nguyen, T., St Martin, S.J., Ou, L., Tom, S., et al. (2018). Dose-Dependent Prevention of Metabolic and Neurologic Disease in Murine MPS II by ZFN-Mediated In Vivo Genome Editing. Mol. Ther. *26*, 1127–1136.

31. Ou, L., DeKelver, R.C., Rohde, M., Tom, S., Radeke, R., St Martin, S.J., Santiago, Y., Sproul, S., Przybilla, M.J., Koniar, B.L., et al. (2019). ZFN-Mediated In Vivo Genome Editing Corrects Murine Hurler Syndrome. Mol. Ther. *27*, 178–187.

32. Sharma, R., Anguela, X.M., Doyon, Y., Wechsler, T., DeKelver, R.C., Sproul, S., Paschon, D.E., Miller, J.C., Davidson, R.J., Shivak, D., et al. (2015). In vivo genome editing of the albumin locus as a platform for protein replacement therapy. Blood *126*, 1777–1784.

33. Szymczak, A.L., Workman, C.J., Wang, Y., Vignali, K.M., Dilioglou, S., Vanin, E.F., and Vignali, D.A. (2004). Correction of multi-gene deficiency in vivo using a single 'self-cleaving' 2A peptide-based retroviral vector. Nat. Biotechnol. *22*, 589–594.

34. Lemansky, P., Bishop, D.F., Desnick, R.J., Hasilik, A., and von Figura, K. (1987). Synthesis and processing of alpha-galactosidase A in human fibroblasts. Evidence for different mutations in Fabry disease. J. Biol. Chem. *262*, 2062–2065.

35. Anguela, X.M., Sharma, R., Doyon, Y., Miller, J.C., Li, H., Haurigot, V., Rohde, M.E., Wong, S.Y., Davidson, R.J., Zhou, S., et al. (2013). Robust ZFN-mediated genome editing in adult hemophilic mice. Blood *122*, 3283–3287.

36. Deveau, H., Barrangou, R., Garneau, J.E., Labonté, J., Fremaux, C., Boyaval, P., Romero, D.A., Horvath, P., and Moineau, S. (2008). Phage response to CRISPR-encoded resistance in Streptococcus thermophilus. J. Bacteriol. *190*, 1390–1400.

37. Mojica, F.J.M., Díez-Villaseñor, C., García-Martínez, J., and Almendros, C. (2009). Short motif sequences determine the targets of the prokaryotic CRISPR defence system. Microbiology (Reading) *155*, 733–740.

38. Chou, S.T., Leng, Q., and Mixson, A.J. (2012). Zinc Finger Nucleases: Tailor-made for Gene Therapy. Drugs Future *37*, 183–196.

39. Miller, J.C., Patil, D.P., Xia, D.F., Paine, C.B., Fauser, F., Richards, H.W., Shivak, D.A., Bendaña, Y.R., Hinkley, S.J., Scarlott, N.A., et al. (2019). Enhancing gene editing specificity by attenuating DNA cleavage kinetics. Nat. Biotechnol. *37*, 945–952.

40. Doyon, Y., Vo, T.D., Mendel, M.C., Greenberg, S.G., Wang, J., Xia, D.F., Miller, J.C., Urnov, F.D., Gregory, P.D., and Holmes, M.C. (2011). Enhancing zinc-finger-nuclease activity with improved obligate heterodimeric architectures. Nat. Methods *8*, 74–79.

41. Miller, J.C., Holmes, M.C., Wang, J., Guschin, D.Y., Lee, Y.L., Rupniewski, I., Beausejour, C.M., Waite, A.J., Wang, N.S., Kim, K.A., et al. (2007). An improved zinc-finger nuclease architecture for highly specific genome editing. Nat. Biotechnol. *25*, 778–785.

42. Paschon, D.E., Lussier, S., Wangzor, T., Xia, D.F., Li, P.W., Hinkley, S.J., Scarlott, N.A., Lam, S.C., Waite, A.J., Truong, L.N., et al. (2019). Diversifying the structure of zinc finger nucleases for high-precision genome editing. Nat. Commun. *10*, 1133.

43. Lino, C.A., Harper, J.C., Carney, J.P., and Timlin, J.A. (2018). Delivering CRISPR: a review of the challenges and approaches. Drug Deliv. *25*, 1234–1257.

44. Flotte, T.R., Afione, S.A., Solow, R., Drumm, M.L., Markakis, D., Guggino, W.B., Zeitlin, P.L., and Carter, B.J. (1993). Expression of the cystic fibrosis transmembrane conductance regulator from a novel adeno-associated virus promoter. J. Biol. Chem. *268*, 3781–3790.

45. Logan, G.J., Dane, A.P., Hallwirth, C.V., Smyth, C.M., Wilkie, E.E., Amaya, A.K., Zhu, E., Khandekar, N., Ginn, S.L., Liao, S.H.Y., et al. (2017). Identification of liver-specific enhancer-promoter activity in the 3′ untranslated region of the wild-type AAV2 genome. Nat. Genet. *49*, 1267–1273.

46. Michalopoulos, G.K. (2007). Liver regeneration. J. Cell. Physiol. *213*, 286–300.

47. Iyama, T., and Wilson, D.M., 3rd (2013). DNA repair mechanisms in dividing and non-dividing cells. DNA Repair (Amst.) *12*, 620–636.

48. Nguyen, G.N., Everett, J.K., Kafle, S., Roche, A.M., Raymond, H.E., Leiby, J., Wood, C., Assenmacher, C.A., Merricks, E.P., Long, C.T., et al. (2021). A long-term study of AAV gene therapy in dogs with hemophilia A identifies clonal expansions of transduced liver cells. Nat. Biotechnol. *39*, 47–55.

49. Bell, P., Moscioni, A.D., McCarter, R.J., Wu, D., Gao, G., Hoang, A., Sanmiguel, J.C., Sun, X., Wivel, N.A., Raper, S.E., et al. (2006). Analysis of tumors arising in male B6C3F1 mice with and without AAV vector delivery to liver. Mol. Ther. *14*, 34–44.

50. Chandler, R.J., LaFave, M.C., Varshney, G.K., Trivedi, N.S., Carrillo-Carrasco, N., Senac, J.S., Wu, W., Hoffmann, V., Elkahloun, A.G., Burgess, S.M., and Venditti, C.P. (2015). Vector design influences hepatic genotoxicity after adeno-associated virus gene therapy. J. Clin. Invest. *125*, 870–880.

51. Rosas, L.E., Grieves, J.L., Zaraspe, K., La Perle, K.M., Fu, H., and McCarty, D.M. (2012). Patterns of scAAV vector insertion associated with oncogenic events in a mouse model for genotoxicity. Mol. Ther. *20*, 2098–2110.

52. Gil-Farina, I., Fronza, R., Kaeppel, C., Lopez-Franco, E., Ferreira, V., D'Avola, D., Benito, A., Prieto, J., Petry, H., Gonzalez-Aseguinolaza, G., and Schmidt, M. (2016). Recombinant AAV Integration Is Not Associated With Hepatic Genotoxicity in Nonhuman Primates and Patients. Mol. Ther. *24*, 1100–1105.

53. Ogawa, K., Hirai, Y., Ishizaki, M., Takahashi, H., Hanawa, H., Fukunaga, Y., and Shimada, T. (2009). Long-term inhibition of glycosphingolipid accumulation in Fabry model mice by a single systemic injection of AAV1 vector in the neonatal period. Mol. Genet. Metab. *96*, 91–96.

54. Yasuda, M., Huston, M.W., Pagant, S., Gan, L., St Martin, S., Sproul, S., Richards, D., Ballaron, S., Hettini, K., Ledeboer, A., et al. (2020). AAV2/6 Gene Therapy in a Murine Model of Fabry Disease Results in Supraphysiological Enzyme Activity and Effective Substrate Reduction. Mol. Ther. Methods Clin. Dev. *18*, 607–619.

55. Ziegler, R.J., Cherry, M., Barbon, C.M., Li, C., Bercury, S.D., Armentano, D., Desnick, R.J., and Cheng, S.H. (2007). Correction of the Biochemical and Functional Deficits in Fabry Mice Following AAV8-mediated Hepatic Expression of alpha-galactosidase A. Mol. Ther. *15*, 492–500.

56. Ziegler, R.J., Lonning, S.M., Armentano, D., Li, C., Souza, D.W., Cherry, M., Ford, C., Barbon, C.M., Desnick, R.J., Gao, G., et al. (2004). AAV2 vector harboring a liver-restricted promoter facilitates sustained expression of therapeutic levels of alpha-galactosidase A and the induction of immune tolerance in Fabry mice. Mol. Ther. *9*, 231–240.

57. Harmatz, P., Lau, H.A., Heldermon, C., Leslie, N., Wong Po Foo, C., Vaidya, S.A., and Whitley, C.B. (2019). EMPOWERS: A phase 1/2 clinical trial of SB-318 ZFN-mediated in vivo human genome editing for treatment of MPS I (Hurler syndrome). Mol. Genet. Metab. *126*, S68.

58. Muenzer, J., Prada, C.E., Burton, B., Lau, H.A., Ficicioglu, C., Wong Po Foo, C., Vaidya, S.A., Whitley, C.B., and Harmatz, P. (2019). CHAMPIONS: A phase 1/2 clinical trial with dose escalation of SB-913 ZFN-mediated in vivo human genome editing for treatment of MPS II (Hunter syndrome). Mol. Genet. Metab. *126*, S104.

59. Donello, J.E., Loeb, J.E., and Hope, T.J. (1998). Woodchuck hepatitis virus contains a tripartite posttranscriptional regulatory element. J. Virol. *72*, 5085–5092.

60. Ayuso, E., Mingozzi, F., Montane, J., Leon, X., Anguela, X.M., Haurigot, V., Edmonson, S.A., Africa, L., Zhou, S., High, K.A., et al. (2010). High AAV vector purity results in serotype- and tissue-independent enhancement of transduction efficiency. Gene Ther. *17*, 503–510.

61. Wright, J.F., and Zelenaia, O. (2011). Vector characterization methods for quality control testing of recombinant adeno-associated viruses. In Methods in Molecular Biology, O.W. Merten and M. Al-Rubeai, eds. (Human Press), pp. 247–278.

62. Wang, A.M., Ioannou, Y.A., Zeidner, K.M., Gotleb, R.W., Dikman, S., Stewart, C.L., and Desnick, R.J. (1996). Generation of a mouse model with α-galactosidase A deficiency. Am. J. Hum. Genet. *59*, A208.

63. Desnick, R.J., Allen, K.Y., Desnick, S.J., Raman, M.K., Bernlohr, R.W., and Krivit, W. (1973). Fabry's disease: enzymatic diagnosis of hemizygotes and heterozygotes. Alpha-galactosidase activities in plasma, serum, urine, and leukocytes. J. Lab. Clin. Med. *81*, 157–171.

64. Mayes, J.S., Scheerer, J.B., Sifers, R.N., and Donaldson, M.L. (1981). Differential assay for lysosomal alpha-galactosidases in human tissues and its application to Fabry's disease. Clin. Chim. Acta *112*, 247–251.